Atmospheric
Chemistry
and Physics
Discussions

Photolytically-Generated Sulfuric Acid and Particle Formation: Dependence on Precursor Species

David R. Hanson[1], Hussein Abdullahi[1], Seakh Menheer[1], Joaquin Vences[1], Michael R. Alves[1,2], and Joan Kunz[1]

5   [1] Chemistry Department, Augsburg University, Minneapolis, MN 55454, USA
     [2] Chemistry and Biochemistry, University of California - San Diego, La Jolla, CA 92093, USA

Correspondence to: D. R. Hanson (hansondr@augsburg.edu)

Abstract. Size distributions of particles formed from sulfuric acid (H_2SO_4) and water vapor in a Photolytic Flow Reactor
10   (PhoFR) were measured with a nano-particle mobility sizing system. Experiments with added ammonia and dimethylamine
were also performed. $H_2SO_{4(g)}$ was synthesized from HONO, sulfur dioxide, and water vapor, initiating OH oxidation by
HONO photolysis. For standard reactant flows and conditions, 296 K, 52 % relative humidity, and a ~40 s residence time,
the calculated concentration of H_2SO_4 peaked at 1.2×10^{10} cm^{-3}, measured particle mean diameter was ~6 nm and total
number density was ~10^4 cm^{-3}. Measured distributions were influenced by molecular clusters at small sizes, less than or
15   equal to 2 nm diameter, but were generally dominated by large particles that are roughly log-normal with mean diameters
ranging up to 12 nm and a relatively constant $\ln\sigma$ of ~0.3. Particle number density and their mean size depended on relative
humidity, HONO concentration, illumination, and SO_2 level. Particle formation conditions were stable over many months.
Addition of single-digit pmol/mol mixing ratios of dimethylamine led to very large increases in number density. Ammonia
at levels up to 2000 pmol/mol showed that NH_3 is less effective than dimethylamine at producing particles. A two-
20   dimensional simulation of PhoFR reveals that H_2SO_4 scales with HONO and its level builds along the length of the flow
reactor. Experimentally, particle growth scaled with HONO, in accord with model-predicted H_2SO_4 levels. Additional
comparison between experiment and model indicates that reaction of HO_2 with SO_2 could be a significant source of H_2SO_4 in
this experiment. The effects of potential contaminants on particle formation rates near room temperature are addressed and
provide context in comparisons with previous experiments. The added-base experimental results provide support for
25   previously published dimethylamine-H_2SO_4 cluster thermodynamics but do not support previously published ammonia-
sulfuric acid thermodynamics.

1 Introduction

Particle formation in the atmosphere has long been studied (McMurry et al. 2005; Kulmala et al. 2004) to ascertain potential
impacts on health (Nel 2005) and on climate processes(IPCC 2013). For example, nano-particles (characterized as < 10 nm
30   in diameter) can have special health effects as their small size allows for efficient transport into lung tissue (Kreyling et al.

2006). They also influence climate by growing to sizes large enough to affect radiative forcing and the properties of clouds. Despite numerous and wide-ranging studies devoted to understanding new particle formation, mechanisms and nucleation rates applicable to many regions of the atmosphere remain uncertain.

5   Sulfuric acid-driven nucleation is a prime source of nanoparticles in the atmosphere (Kuang et al. 2012; Sipilae et al. 2010) thus it is the starting point for many laboratory studies.   Previous work on particle nucleation in the binary (water-sulfuric acid) system (Kirkby et al. 2011; Ball et al. 1999; Zollner et al. 2012; Ehrhart et al. 2016; Yu et al. 2017) have concluded that binary nucleation can be significant at low temperatures such as at high latitudes and in the upper troposphere. The sulfuric acid/water binary system also serves as an important baseline diagnostic for comparing experimental results. Finally, nanoparticle growth by sulfuric acid and water vapors is of interest as well as uptake of oxidized organic compounds

10   by acidic nanoparticles. Good knowledge of the formation and stability of binary nano-particles is needed to understand their subsequent growth via other compounds.

Previous laboratory studies of nucleation in the binary system diverge widely, especially for results taken at or near room-temperature, and experimental details may significantly affect results. For example, does it matter if H_2SO_4 is provided by a bulk or photolytic source or from which photolytic precursor: O_3, H_2O_2, H_2O, etc. (Sipilae et al. 2010; Berndt et al. 2008;

15   Laaksonen et al. 2008) ?   What are the limitations imposed by particle detector characteristics as well as cluster/particle wall losses (McMurry 1983; Kürten et al. 2015) ?   How well-determined are the concentrations of H_2SO_4 (Sipilae et al. 2010; Jokinen et al. 2018) ?

A prime concern is whether contaminants are present at abundances significant enough to influence particle formation rates. For example, Zollner et al. (2012) argued that a 10^{-14} mixing ratio of methylamine could have affected their binary system

20   measurements; Glasoe et al. (2015) carried this argument further and estimated that contaminant dimethylamine mixing ratios were less than 10^{-15}. Kirkby et al. (2011) and more recently Kurten et al. (2016) estimate ammonia contaminant levels of 4-to-10 pptv NH_3 for their experiments performed at 292 - 298 K. Recently, Yu et al. (2017) reported upper limits for NH_3 and dimethylamine of 23 and 0.5 pmol/mol (pptv), respectively. Impurity dimethylamine at this level would very likely overwhelm binary system nucleation which underscores the importance of assessing potential contaminants.

25   Here we describe an apparatus and results from experiments on the formation of sulfuric acid nanoparticles from photolytically-generated sulfuric acid vapor (the $OH+SO_2$ photochemistry initiated with HONO photolysis at ~350-to-370 nm). Although nitrous acid is considered an important contributor to OH radical formation in many situations (Sörgel et al. 2011), little has been done to understand its photolysis that leads to sulfuric acid formation and new particle formation. We also studied the effects of adding ammonia or dimethylamine; both are known to greatly enhance particle production rates

30   (Almeida et al. 2013; Glasoe et al. 2015; Yu, McGraw, and Lee 2012; Ortega et al. 2012; Nadykto and Yu 2011). Finally, the experimental results are compared to simulations of the flow reactor that couple the flow with photo-chemical kinetics and an acid-base particle formation scheme.

2 Methods

The Photolytic Flow Reactor (PhoFR) is a vertically-aligned cylindrical glass tube with an inner diameter of 5.0 cm, a length of ~130 cm, a volume of approximately 2.5 L and topped with a 23 cm conical glass piece with several flow inlets (Fig. 1a). In the course of this work, a Teflon screen was positioned between the cone and the flow reactor to calm the jetting from the

5   inlets. A ~ 105 cm portion of PhoFR is jacketed and kept at a constant temperature, typically 296 K, by circulation of thermostated water. The main flow of gas was nitrogen from a liquid nitrogen gas-pack and the total flow rate was 2.9 sLpm (standard L / min, 273 K and 1 atm). The flow contained small amounts of SO_2 and HONO, typically a few and 0.02 ☐mol/mol (ppmv), respectively, and up to several % water vapor; relative humidity was set by sending a portion of the flow over a heated water reservoir and then through a thermostated, vertically-aligned tube that removed excess water vapor.

10   Total pressure was slightly above ambient, ~ 0.98 atm: gauge pressure was monitored continuously and it was typically 0.001 atm. The oxygen level from the liquid nitrogen, stated to be 10 ppmv or less, was apparently sufficient for the subsequent oxidation chemistry - noting little differences in particle size additions upon adding several % O_2 to the flow.

Entering gas flows were monitored and set by mass flow meters under computer control. Typical flows for baseline conditions in sLpm or sccm (standard cm^3 / min, 273 K, 1 atm) were dry gas at 1.4 sLpm, fully humidified air at 1.5 sLpm,

15   HONO-laden (~15 ppmv, μmol/mol) N_2 flow at 4.2 sccm, and SO_2-laden flow at 32 sccm (1500 ppmv SO_2-in-N_2). These baseline conditions help diagnose the long term stability of the system. The baseline number densities of SO_2 and HONO in the flow reactor (accounting for dynamic dilution) are 4×10^{14} and 6×10^{11} cm^{-3}, respectively. The conical top section and the bottom 20 cm where aerosol was sampled were not insulated or thermo-regulated.

The SO_2-in N_2 mixture (Minneapolis Oxygen) was reported (Liquid Technologies Corporation, EPA Protocol) to contain

20   1500 ppmv SO_2 +/- 10%. Water vapor was taken from a gently heated ~500 mL volume of deionized water (Millipore) that also contained a few grams of concentrated sulfuric acid to suppress potential base contamination from the bulk water. This humidified flow then passed through 80 cm of vertically-aligned Teflon tubing (~6.2 mm ID) held at the temperature of the flow reactor.

Photolyte HONO was continuously produced (Febo et al. 1995) by flowing nitrogen laden with ~15 ppmv HCl vapor into a

25   small (25 mL) round-bottom flask containing 1-2 grams of powdered NaONO(s), held at 40-50°C (Fig. 1b). HONO vapor and co-product NaCl(s) are produced in a classic double-displacement reaction. The powder could be very slowly mixed with a small (1 cm long) stir bar and results generally did not depend on whether the powder was stirred. Periodic gentle shaking of the flask usually led to only temporary changes in particle number densities.

The HONO level exiting the generator is likely to be equal to the HCl level entering it. The HCl-generator and a water vapor

30   pre-saturator were temperature-controlled at typically 20 °C. A saturated (~6 m, molal) NaCl aqueous solution in the pre-saturator yields a relative humidity of 76 % in the flow: a stable amount of water vapor stabilizes the solution in the HCl-generator, which contains a solution with a 2-to-1 mole ratio for NaCl to H_2SO_4. The HCl-generator solution was prepared initially with concentrations of 3.5 m NaCl and 1.75 m H_2SO_4 and calculations (Wexler and Clegg, 2002; Friese and Ebel,

Atmospheric
Chemistry
and Physics
Discussions

2010) result in an HCl vapor pressure of 9.3×10^{-6} atm. UV absorption measurements to determine the HONO level in this flow are described in the Supplement and results indicate that the source has a HONO level of about 1.5×10^{-5} atm. This suggests that the HCl-generator's HCl vapor pressure is slightly larger than the calculated value. While the water vapor pre-saturator minimized loss of water from the HCl-generator, small temperature differences between these two vessels can

5   introduce variability and possibly a bias.

Four black lights that have a UVA spectral irradiance centered at 360 nm illuminated about a 115 cm length of the jacketed flow reactor from a distance of about 15 cm from the reactor center. A rough estimate of the fluence (5×10^{15} photons cm^{-2} s^{-1}) indicates a photolysis rate of approximately 10^{-3} s^{-1} for HONO. Described in the Supplement is an experiment where production of methylvinylketone and methacrolein from the oxidation of isoprene was monitored, yielding an estimate

10 (along with the 15 ppmv HONO level discussed above) for the HONO photolysis rate of 8×10^{-4} s^{-1}.

H_2SO_4 is formed via (i) OH produced via HONO photolysis, (ii) OH addition to SO_2, (iii) H-atom abstraction by O_2 and (iv) reaction of SO_3 with H_2O molecules (Lovejoy et al.) The HO_2 and NO radicals generated in this process can react together and generate an additional OH radical. When SO_2 is present at a few ppmv, the dominant loss for OH is OH + SO_2: a pseudo-first-order loss rate coefficient is given by $[SO_2]*k_{OH+SO2} = 4 \times 10^{14}$ cm^{-3} * 8.9×10^{-13} cm^{3}s^{-1} = 360 s^{-1}. With this SO_2

15 baseline level, OH reacts with HONO only about 1 % of the time: an OH first-order loss rate coefficient is ~3 s^{-1}, from $[HONO]*k_{OH+HONO} = 5 \times 10^{11}$ cm^{-3} * 6×10^{-12} cm^{3}s^{-1}. For low SO_2 levels, loss of OH due to reaction with HONO can be significant.

H_2SO_4 levels build as the flow moves down the reactor, forming H_2SO_4 molecular clusters and these clusters grow into stable particles. These particles accumulate enough material, primarily H_2SO_4 and H_2O, to grow to several nm in diameter.

20 Growth due to OH or HO_2 uptake followed by reaction with absorbed SO_2 may also contribute to growth.

Particles were sampled on axis at the exit of the flow reactor, about 120 cm from the conical inlet, with a custom-built mobility-sizing and counter system designed for nanometer-sized particles. Briefly, size-classified particles (Am-241 charger and a TSI 3085 nanoDMA) were detected with a diethyleneglycol (DEG), sheathed condensation particle counter (CPC) in tandem with a butanol-based CPC (Jiang et al. 2011). This system is denoted 'DEG system' in this study. The

25 DEG CPC was operated with a saturator temperature of 57°C, a condenser temperature of 20°C, 0.36 L/min condenser flow and 0.07 L/min capillary flow. The nanoDMA was operated with 2 L/min aerosol-in and monodispersed-out flows and a 13 L/min sheath flow, as in Glasoe et al.

For a few experiments, ammonia or dimethylamine as trace gases were added through a port at the top of the flow reactor. Their sources were permeation tubes, and 100s and single-digit pptv levels could be set by either single- or double-stage,

30 respectively, dynamic dilution systems (Freshour et al. 2014; Glasoe et al. 2015). Ammonia was used in the single-dilution system and dimethylamine was dedicated for use in the double-dilution system. Permeation rates were determined periodically by re-directing the base-laden flow through an acidic solution and monitoring the change in pH over time (Freshour et al., 2014).

Atmospheric
Chemistry
and Physics
Discussions

2.1 Model

The 2-dimensional model of the flow reactor incorporating the photochemical kinetics of H_2SO_4 formation was built on a previous model of acid-base molecular cluster formation which was fully corroborated against a commercial computational fluid dynamics simulation (Hanson et al. 2017). The flow profile can be set to either plug or fully-developed laminar,

5   clusters up to ten H_2SO_4 and base molecules can be simulated. The 2D model here incorporates the detailed photochemistry in our experiment, from the production of OH through its reactions with SO_2 as well as with HO_2, NO, NO_2, HONO, HNO_3, H_2O_2 etc. The acid and base species and all molecular clusters as well as OH are lost on the walls limited only by diffusion. The model reacts, convects and diffuses all reactants and products and yields the abundance of H_2SO_4 molecular clusters, the largest clusters are then correlated to the abundance of experimentally determined particles (Panta et al. 2012; Hanson et al.

10   2017). Coagulation is only crudely implemented, but these cluster-cluster interactions are not significant for most of the conditions of the present work. Also, the largest clusters can be grown to very large sizes via uptake of H_2SO_4 (and H_2O) assuming no loss. Further analysis of cluster growth and loss processes, including growth-only for clusters larger than 10 H_2SO_4 molecules, is presented in the Supplement.

Ammonia or dimethyl amine could be included at a trace level with the flow entering the simulated reactor whereupon acid-

15   base clustering commences and thus particle formation (note that base is also lost to the wall, limited by diffusion). The photochemistry is described in detail in the Supplement and the acid-base clustering reactions are described in detail in Hanson et al. 2017 along with thermodynamic schemes for clusters of the bases with sulfuric acid (those used here are primarily the NH3_I and DMA_I schemes from that work.)

3 Results and Discussion

20   #### 3.1 Particle formation evaluation.

The stability of particle formation conditions over several months is demonstrated by presenting the number and the average size of particles for baseline conditions. In the next section, the modeled photochemistry for baseline conditions is presented to provide baseline particle formation conditions within PhoFR. Here, we also discuss how the size distributions were analyzed. In subsequent sections, these analytical devices will be applied to the results of experiments where reactant levels

25   were varied.

Shown in Figure 2 are results over a 4 month period for baseline conditions: 52 % relative humidity (RH), 296 K, total flow of 2.9 sLpm, and a flow of N_2 through the HONO source, Q_4, of 4.2 sccm. The data was binned according to the flow of the SO_2 mixture, Q_1, either 4 sccm or > 20 sccm. The abundance of HONO is 20 ppbv and SO_2 is either 2 ppmv or >10 ppmv. Fig. 2a shows the total particle number density, N_p, and Fig. 2b shows representative particle size distributions - corrected for

30   size-dependent diffusion losses in CPC transport and inlet lines. N_p was determined by summing the particle concentrations with D_p of ~2.4 nm and larger. The two smallest diameter concentrations are not included because they have large

Atmospheric
Chemistry
and Physics
Discussions

uncertainties due to large corrections applied to low count rates; furthermore, a mobility diameter of 2.4 nm is a local minimum for most of the size distributions.

The measured size distributions are governed by the interplay between the spatial distribution of $[H_2SO_4]$, whether base is added, and the nature of potential contaminant species. For example, the small- and the middle-sized particles decrease considerably between Feb. 23rd and May 15th (Fig. 2b) which is probably due to a decrease in particle-enhancing contaminants. Yet the concentrations of the largest particles are comparable in these two data sets: in other words, the leading edges of the distributions are similar. The largest particles must originate at the top of the reactor, having the highest overall exposure to H_2SO_4. These so-called leading-edge particles are the focus of our analysis.

The leading-edge particles are greatly enhanced when base was added, whether ammonia or dimethylamine. In these cases, the leading-edge particles are prominent in the distributions and are described by log-normals (see the distributions presented below). The leading-edge volume-mean diameters for the added-base experiments are similar to those of the no-added base distributions. So we propose that the leading-edge particles are indicative of the nucleation conditions at the top of PhoFR. In the Supplement is more discussion of the leading-edge mode of the particle size distributions, plots of modeled distributions and experimental leading-edge mode diameters (D_{le}) over time.

The high SO_2 data (Fig. 2a) exhibits an N_p that averages about 2×10^4 cm^{-3} since late February; also the leading edge of the size distributions (Fig. 2b), fit to log-normal functions, indicate mode diameters of about 6 nm with $\ln\sigma$ values of ~0.35. The large drop in N_p on the 23rd of February is due to a Teflon mesh (ultrasonically cleaned and soaked overnight in a dilute sulfuric acid solution) placed between the cone and the flow reactor. The mesh limits backstreams from the illuminated section that may introduce H_2SO_4 and thus nucleation in the cone. Ever since this big drop in N_p, a trend in N_p can be discerned in Fig. 2a that is consistent with the changes with time of the size distributions in Fig. 2b. On the other hand, mode diameters (presented in the Supplement) indicate that D_{le} is roughly constant from January to May.

Since changes in D_{le} are small or negligible, the growth conditions in PhoFR must be stable during this 4-month time period. The cumulative exposure of particles to H_2SO_4 as they travel down PhoFR is constant, indicating that the UV flux and reactant concentrations are also. The decrease in large particle numbers during this time likely indicates an increase in the purity of the system, for example a decrease in contaminant base levels entering the flow reactor. An increase in the cleanliness of the system could also be due to acid buildup on surfaces, potentially binding base-emitting contaminants. The changes in the distributions over 2.5 months (Fig.2b) are due to decreases in particles in the middle of the distribution. Based on their size, these particles were nucleated downstream of where the leading edge particles are. The flow reactor wall may accumulate enough acid that may tie up a purported contaminant responsible for the mid-sized particles.

3.1.1 Simulated reactant distributions

Shown in Fig. 3 are the results of a simulation using the 2D model that shows centerline concentrations of the gas-phase species and two molecular clusters. In order of abundance at the end of the reactor: On the left axis, H_2SO_4, NO_2, NO, HO_2, H_2O_2, HO_2NO_2 and NH_3; and on the right axis, OH, $(H_2SO_4)_2NH_3$ and 100 times the SA_8 cluster abundance. This simulation

was performed with [HONO] = 5×10^{11} cm^{-3}, simulating an experiment with Q_4 = 4 sccm. These conditions are close to those for the size distributions depicted in Fig. 2b.

Sulfuric acid rises steadily and reaches 1.2×10^{10} cm^{-3} by the end of the lighted section that extends from 0 to 110 cm. NH$_3$ was introduced at the inlet at a level of 70 pptv which drops with axial distance due to wall loss: its concentration drops to

5   ~20 % of the inlet value by 40 cm. The effect of added base on particle formation is primarily at the top of the reactor despite the lowest sulfuric acid abundances there. The remaining 2/3 of the reactor has the highest sulfuric acid levels: over the distance 40 to 125 cm, [H$_2$SO$_4$] averages about 8×10^9 cm^{-3}.

This crude partitioning of the reactor is somewhat arbitrary but it provides a point of view for discussing the experimental results. Furthermore, this point of view is congruent with the experimental finding that a large particle mode at the leading

10   edge of the size distributions is discernible, especially so when base was added. So although clusters are formed and particles are nucleated along the length of the reactor, we seek to explain only the largest of them.

With this perspective, we can estimate the growth of the leading-edge particles due to their accumulating H$_2$SO$_4$ and H$_2$O (assuming no evaporation) as they traverse the bottom 2/3 of the flow reactor. Using centerline values, an increase in particle diameter of 4.8 nm is estimated as they travel from 40 to 125 cm, using the bulk approximation to calculate the

15   increase in diameter (Verheggen and Mozurkewich, 2002; Wexler and Clegg, 2002). Modeled particles that contain up to 250 H$_2$SO$_4$ molecules yield particle size distributions in agreement with this estimate from bulk properties (see the Supplement).

The behavior of the truncated clusters shown in Fig. 3 provides some justification for partitioning the reactor into a top 1/3 and a bottom 2/3. The abundance of (H$_2$SO$_4$)$_2$NH$_3$ peaks at about 50 cm indicating that nucleation involving base has

20   reached its peak. The accumulation cluster (that was allowed to build up at 8 SA molecules but no further and with no SA evaporation) tells a similar story regarding this partitioning where its abundance levels off in the lower section of the reactor. Its behavior in the middle of the reactor, a lag in its abundance profile compared to the SA$_2$NH$_3$ cluster, indicates that some catching up is needed to grow the clusters to 8 SA molecules. The increase in the abundance of these clusters with Z reaches a maximum near 60 cm. This indicates that the partitioning is a decent rhetorical tool for discussing the results and for

25   drawing broad conclusions.

3.2 Variation of Np, Dp with [reactant]

3.2.1 Variation of HONO with no added base.

Depicted in Fig. 4a are representative particle size distributions as a function of N$_2$ flow through the HONO source, Q_4, a proxy for HONO abundance. Q_4 was varied from 1.6 to 5.3 sccm while the abundances of the other reactants were held

30   constant. The size distributions are strongly dependent on HONO over this range, with concentrations increasing by a factor of ~ten at small sizes and the large particle abundance by a hundred-fold. Log-normal distributions are also shown as the dashed lines in the figure with leading-edge mode diameter D$_{le}$ and lnσ noted in the legend. The log-normals shown in the

Atmospheric
Chemistry
and Physics
Discussions

figure were not those from the fitting procedure (see the Supplement for more discussion of the fitting procedure) because two of the fits failed. For a consistent presentation, $\ln\sigma$ was fixed and each log-normal was adjusted visually to best cover the four or five points nearest the peak of each distribution. N_p (Fig. 4b) and the volume-mean diameter of the leading edge mode, $D_{V,le}$ (Fig. 4c) are plotted vs. Q_4 and N_p has a power-dependence on Q_4 of about 4 while $D_{V,le}$ increases linearly over

5   most of this range.

It is reasonable to assume that the HONO concentration in PhoFR is linearly proportional to Q_4, the nitrogen flow through the HONO source. The data in Fig. 4c shows that $D_{V,le}$ scales approximately linearly with Q_4 up to about 7 sccm, suggesting that particles exposure to H_2SO_4 is also linear over this range. The departure from linearity is noticeable in Fig. 4c and is probably affected by the inability of the fitting process (see Supplement) to yield leading edge log-normal distributions at

10   low values of Q_4 (indeed about half failed for $Q_4 \leq 2.2$ sccm) and scavenging of H_2SO_4 by particle surface area at the large N_p that develops at high number densities and large sizes when Q_4 is 8 to 10 sccm.

A power dependence of 5 for N_p on H_2SO_4 was exhibited for the H_2SO_4-H_2O binary system (Zollner et al. 2012) which is somewhat larger than that exhibited in Fig. 4b; other bulk experiments have power dependencies on H_2SO_4 that range up to ~20 (Wyslouzil et al. 1991; Viisanen et al. 1997). Yet the CLOUD experiment (Kurten et al. 2016), also with photolytic

15   generation of H_2SO_4, shows a power dependency of 3.7 at 292 K for [H_2SO_4] concentrations from 3×10^8 to 1.5×10^9 cm^{-3}. An ammonia-contaminant abundance of 4 pptv was stated to apply to those results.

Experimental results (Glasoe et al. 2015; Almeida et al. 2013) show that power dependencies on H_2SO_4 are affected when a base is present. The presence of an impurity base compound probably affected our experimental results. It may be due to two sources: (i) contaminant entering with the flows and (ii) contaminant emanating from internal surfaces. The added base

20   experiments have more discussion on this topic but we note here that our system is slowly cleaning up over time.

Particles grow due to uptake of H_2SO_4 and H_2O: the estimate from the H_2SO_4 profile from the model simulation discussed above suggests an increase in diameter of about 4.8 nm for a Q_4 of 4.0 sccm. The data in Fig. 4c show that the volume mean diameter is about 6 nm at this HONO level, which is consistent with that estimate. The agreement improves considering that nascent particles must attain a certain size to become stable, roughly 1.3 nm diameter or larger (large enough such that

25   evaporation becomes negligible). There is also a 0.3 nm difference between mobility and volume/mass diameters. Presented in the Supplement are simulated particle size distributions for $Q_4 = 2$ sccm that peak at 3.7 nm in good agreement with measurements.

3.2.2 SO_2.

Particle size and number density were found to depend on SO_2 abundance. Shown in Figs. 5 (a) and (b) are plots of N_p and

30    $D_{V,le}$ (volume mean diameter of the leading-edge mode) vs. the flow rate of the SO_2 mixture, Q_1. HONO source flow rate Q_4 was 4.2 sccm for this data. Despite its scatter, the data show the SO_2 level affects both the number of large particles and their size, $D_{V,le}$: both increase with [SO_2] and begin to level-off at high [SO_2]. This behavior is expected as the SO_2 abundance must be high enough to ensure it scavenges all of the OH and beyond that there should not be much effect.

However, a set of simulations that includes a reaction between HO_2 and SO_2 are shown as the lines in Figs. 5. Note that a level of 70 pptv of NH_3 entering the flow reactor was included. The simulated size is given by the growth estimate from the simulated H_2SO_4 profile plus an initial size of 1 nm and the mobility-diameter to mass-diameter offset of 0.3 nm (de La Mora et al.) The experimental results show increases with SO_2 that are roughly in line with the model simulations. Without

5   a reaction between HO_2 and SO_2, the model shows small increases in N_p (40 % vs. 250 % with the reaction) and size (10% vs. 20 % with the reaction) as SO_2 was increased from 2 to 16 pptv.

The simulation assumed a value of 3×10^{-17} cm^3/s for $k_{HO2+SO2}$. There are disagreements in whether HO_2 reacts with SO_2 as well as potential end products (Chen et al. 2014; Kurten et al. 2011); we assumed H_2SO_4 and OH. Published values for this rate coefficient range from upper limits of 1×10^{-18} cm^3/s (Graham et al. 1979) and 2×10^{-17} cm^3/s (Burrows et al. 1979), to a

10   value of 8×10^{-16} cm^3/s (Payne et al. 1973). A heterogeneous reaction occurring in the particles involving SO_2 would help explain the dependence of $D_{V,le}$ on SO_2 abundance while leaving N_p undisturbed.

The dependencies upon SO_2 were much smaller when minute amounts of dimethylamine were included in the model. Low levels of (0.003 pptv) dimethylamine gave simulated N_p in the 10^4 cm^{-3} range but at this level its ability to influence the change in N_p with H_2SO_4 was limited due to being scavenged by clusters. This was also observed in simulations where

15   HONO was varied in the presence of 0.005 pptv dimethylamine (see the Supplement). This suggests that a potential contaminant in our system is not a strong nucleator like dimethylamine.

3.2.3 Added ammonia.

Shown in Fig. 6 is the number of large particles vs. HONO flow rate taken with and without NH_3 addition. The level of added NH_3 when fully mixed and without any loss to the wall would be 230 pptv. With data for nominal conditions for

20   comparison, the effect of 230 pptv NH_3 on the number of large particle abundance is significant, about a factor of 5, a factor that does not significantly depend on the level of HONO and thus H_2SO_4 present in the flow reactor. Variation of D_{le} as HONO was varied is shown in the Supplement and adding base results in an increase of D_{le} of about 20%. The shift in the distributions to slightly larger sizes could be due to particle formation occurring slightly upstream of that in the absence of added NH_3. Nevertheless, the leading-edge mode of the size distributions are distinct in Fig. 6(b): even the lowest Q_4 in 6(b)

25   can be fit by a log-normal function.

Previous work has shown large increases in N_p when ammonia was added to a (nominally clean) binary sulfuric acid-water nucleating system. For example Ball et al. (1999), Zollner et al. (2012), and Glasoe et al. (2015) observed factors of 10-to-1000, ~1000, and 10^6 for ammonia levels of a few pptv, 25 pptv, and 55 pptv, respectively. Kuerten et al. (2016) presented the CLOUD experiment data in a comprehensive manner and showed that a factor of about 100 increase in particle

30   production was observed upon addition of several hundred pptv NH_3 at 292 K and an $[H_2SO_4] = 1.5 \times 10^8$ cm^{-3}.

Simulations are shown in the Supplement with two different NH_3 levels (70 and 300 pptv) that mimicked the Np vs. Q_4 data remarkably well (70 pptv NH_3 for the no-added base and 300 for the added base case). Dimethylamine levels at 0.003 pptv yielded N_p in the range of the experiment base suggesting that very small amounts of a contaminant can influence binary

Atmospheric
Chemistry
and Physics
Discussions

nucleation experiments. An amide may be consistent with the experiment: it is intermediate in strength (Glasoe et al. 2015), stronger than ammonia but not so strong that scavenging could be a major loss process.

3.2.4 Variation of N_p with added NH$_3$ level.

Shown in Figs. 7 are the total number of particles plotted as a function of added NH$_3$ levels for a fixed amount of HONO: (a)
5   Q_4 = 4.3 sccm and (b) Q_4 = 2.2 sccm. The red squares at nominally zero NH$_3$ represent the range of data obtained without added base. There are large effects on N_p due to the addition of NH$_3$ at the top of the reactor, up to a factor of ten for both sets of data. At high NH$_3$ levels (or prolonged exposure) particles counts rose dramatically. This is demonstrated in the Supplement with measurements on days when 2000 pptv NH$_3$ was added.

The large variability in Figs. 7 mirrors the underlying variability in N_p without added NH$_3$ (Figs. 4b and 5a). Yet, within the
10   scatter of the measurements the dependence of N_p upon NH$_3$ can be approximated as linear. This is a smaller dependence than the 1.6 power dependence found in the bulk-source experiments of Glasoe et al. (2015). A linear dependence is similar to other photolytic H$_2$SO$_4$ production experiments, the flow reactor experiments of Benson et al. (2011) and Berndt et al. (2010), and the 292 K CLOUD chamber experimental results (Kuerten et al. 2016; Kirkby et al. 2011).

Simulated N_p are shown in Fig. 7a for two different thermodynamic schemes (Hanson et al., 2017); both clearly indicate a
15   stronger dependence on NH$_3$ than is exhibited in the experimental results. Failure to mimic the experimental results can be due in part to poor representation of the actual flow in the simulations, however inaccurate thermodynamics are probably the dominant contributor. We had concluded (Hanson et al., 2017) that NH3_II was better than NH3_I based on comparisons to the experimental data of Glasoe et al. (2015). The comparison shown in Fig. 7a indicates that neither satisfactorily represents the full range of the data with NH3_II having particularly overly strong binding free-energies while, relatively
20   speaking, NH3_I is a better approximation of the NH$_3$-H$_2$SO$_4$ cluster binding energies for the present conditions.

3.2.5 Water variation and addition of dimethyl amine.

Shown in Fig. 8 are the N_p and D_{le} vs. humidity, calculated from the flow rate of the humidified nitrogen. Total flow rate, HONO, and SO$_2$ levels were kept constant; the humidified flow rate was varied from 0.5 to 2.4 sLpm. Although the overall data is phenomenologically exponential (see the fit in the figure), over limited ranges the data exhibits power dependencies.
25   The power dependence of N_p on RH is between 4 and 6 while $D_{V,le}$ varies from 5 nm to about 10 nm; there appears to be a rise in both above 80 % RH. A strong dependence of the number of particles on RH is expected for the binary sulfuric acid water nucleating system, and the power dependence here lies at the low end of range (5-to-9) reported by Zollner et al.

A set of data with 2-to-5 pptv dimethylamine added is shown as the diamonds. There is much less water dependence (approximately linear) when dimethylamine is present which is consistent with theoretical notions (Almeida et al. 2013;
30   Henschel et al. 2016). This indicates that clusters that lead to large particles are not particularly sensitive to H$_2$O when dimethyl amine is present, because the amine is a much better base than H$_2$O and nucleation associated with a strong acid-

base interaction is preferred. This postulate has been elucidated in previous publications (e.g. Kurten et al. 2008; Coffman and Hegg 1995).

Supposing there is dimethylamine-type base contaminant in the putatively base-free experiments (solid squares), it clearly does not reach the single digit pptv level for baseline 52 % RH conditions. Indeed, as shown in the Supplement, simulated

5   particle number densities with a level of 0.003 pptv dimethylamine entering the flow reactor were consistent with the 52% RH, Q_4=4 sccm results. A set of simulations were run from 0.005 up to 2 pptv dimethylamine and predicted N_p scaled linearly with base level. At the 2 pptv level, an N_p of about 10^7 cm^{-3} was predicted while experimental N_p is 3×10^6 cm^{-3}. Note that an N_p at the 10^7 cm^{-3} level will be significantly affected by coagulation which is not well captured in the simulations.

10 ### 3.2.6 Variations of dimethylamine and HONO.

Shown in Fig. 9 are measured size distributions with varying levels of added dimethylamine. The effect on the number of particles is large and even the smallest particles (mobility diameter of 1.7 nm) increased by about 3 orders of magnitude. The zero-added base data between these runs might be affected by dimethylamine holdover but this appears to be small: the N_p are within a factor of two of the Q_4=2.2 sccm data in Fig. 4a. It is clear that more dimethylamine leads to more particles,

15 with N_p increasing approximately linearly with dimethylamine abundance. Note that the leading edge of the distributions is clearly the dominant mode for these conditions. The D_{le} does not change significantly with the amount of added dimethyl amine (see the legend for values of D_{le} and $\ln\sigma_{le}$).

Depicted in Fig. 10 are results from an experiment where HONO, Q_4, was varied (and thus H_2SO_4) in the presence of 2 pptv (+100/-50%) dimethylamine. Interestingly, the number of particles is not particularly sensitive to H_2SO_4 above $Q_4 = 2.7$

20 sccm while their size is linearly dependent on Q_4. The model indicates a leveling off in the calculated N_p as Q_4 increases (see the Supplement) which appears to be due to scavenging of the amine by particles. Another contributing factor to an insensitivity of particle number concentrations to H_2SO_4 is particle-particle collisions. A rough estimate of these effects, assuming a coagulation rate coefficient of 2×10^{-9} cm^3/s, for an N_p of 4×10^6 cm^{-3} is $2 \times 10^{-9} \times (4 \times 10^6)^2 = 3 \times 10^4$ cm^{-3} s^{-1} ; multiplying by a 30 s residence time and roughly 1×10^6 cm^{-3} would coagulate. This rough estimate suggests the effect

25 should be properly evaluated, particularly for the data presented in Fig. 9. Note also that these are small sets of data and for Fig. 10 base was added at a level that challenges the lower range of the dynamic dilution system.

Model simulations with DMA_I thermodynamics (Hanson et al. 2017) at $Q_4 = 2$ sccm with dimethylamine at levels of 5 and 10 pptv predict N_p of 5×10^6 cm^{-3} and 1×10^7 cm^{-3}, respectively. These compare favorably with the measured N_p at 5 and 10 pptv of 2.5 and 5×10^6 cm^{-3}, respectively. The modeled values would be reduced with a proper treatment of particle-particle

30 collisions. Nonetheless, the thermodynamic scheme DMA_I yields cluster concentrations that are consistent with the measured N_p and its trends with dimethylamine level. Scheme DMA_I was able to mimic the dimethylamine-H_2SO_4 data of Glasoe et al., tying that data to the present data.

Since effects due to adding dimethylamine at the single-digit pptv level are large, it would be desirable to experimentally investigate amine additions at lower levels. With the current dynamic dilution system base additions at levels lower than a few pptv are swamped by the precision uncertainty in flowmeter readings. More results from these types of experiments await further improvement in the dimethylamine delivery system.

5 **3.3 Comparison to previous results.**

A number of previous results are compiled along with the present measurements in Fig. 11 for nominally base-free conditions. The present results are assigned the simulated H_2SO_4 value in the center of the reactor and at 30 cm into the illuminated region. The nucleation rate J was taken to be N_p divided by the time the center of the flow travels from 20 to 40 cm, 4 s. This time is presumed to apply for the nominally clean conditions here. On the other hand, with base added

10 intentionally, significant nucleation may also occur in the 0 to 20 cm region where base abundance is high. Uncertainties in J are probably on the order of a factor of 2. Uncertainty in H_2SO_4 is about a factor of two, based on the calculated values at 15 and 60 cm, which are -49 and +106 %, resp., from the 30 cm value. The radial profile of H_2SO_4 at 30 cm axial distance is flat from the center out to a radius of 1.7 cm.

The previous experimental data in Fig. 11 were taken over a range of temperatures, 288 to 300 K, and relative humidities,

15 2.3 to 75 % RH; conditions indicated in the legend. The present results extrapolate to rates that are in fair agreement with Benson et al. 2009 and much of the CLOUD data set (Kirkby et al. 2011; Kurten et al. 2016) except for the 40 % RH at 298 K data. The bulk-source H_2SO_4 data reported by Zollner et al. is included for reference; it was corrected from 38% RH to 52 % RH, increasing by about a factor of 5 using a RH^5 dependency. The difference between the bulk-source and present photolytic H_2SO_4 is about 4 orders of magnitude; the Kurten et al. (2016) 40 % RH data is closest to this set of bulk data,

20 within about two orders of magnitude.

There is apparent agreement of several data sets for H_2SO_4 concentrations of 10^8 to 10^9 cm^{-3}: our lowest J (and the extrapolation of our data, dotted line), Yu et al. (2017), Benson et al. (2009), Kurten et al. (2016) and Kirkby et al. (2012) but it is complicated by the wide range of relative humidities: 2.3 % RH up to 75 % RH. Lack of experimental water dependencies and assessment of base-levels makes drawing conclusions fraught with difficulty. Nonetheless, it is interesting

25 that the dependencies of J on sulfuric acid level are similar in many of these studies. This suggests there is an underlying similarity in particle formation conditions such as contaminant identity and level (which seems unlikely) or the critical cluster's H_2SO_4-content is not particularly sensitive to the type or abundance of the contaminant.

4 Summary

We presented a new experimental apparatus for studying particle formation involving photolytically-formed H_2SO_4 vapor

30 and results show the system is reproducible and responds to changes in water, HONO and SO_2 concentrations largely as expected. Modeled particle formation rates could be made congruous with experimental observations by including either

Atmospheric
Chemistry
and Physics
Discussions

dimethylamine at a level of 3×10^{-15} mole fraction or NH_3 at a level of $\sim10^{-10}$ mole fraction. Also, the dependence of N_p on SO_2 level was best explained by a reaction between HO_2 and SO_2 that yields (ultimately) H_2SO_4 and OH with a rate coefficient of 3×10^{-17} cm^3/s.

Comparison of the present results to other photolytic H_2SO_4 experiments yields several suppositions. Their divergence from
5   the bulk-source data of Zollner et al. suggests these experiments are not clean enough and/or they are subject to an unknown reaction or photochemistry. The similarity of the present results to those of Benson et al. (2009), Kirkby et al. (2011), Kurten et al. (2016) and Yu et al. (2017) suggests a common element that affects nucleation beyond what bulk-source H_2SO_4 experiments reveal. The outlier results of Berndt et al. (2010, 2014) and Benson et al. (2011) may suffer from relatively high level of contaminants: Berndt et al. (2014) suggested that a pptv-level of amine could have been present in their experiment.
10   As can be seen in Fig. 11, there is a remarkable agreement of the H_2SO_4 power dependencies for Kirkby et al. (2011), Yu et al. (2017), and the present results. This may be due to a similarly-sized critical cluster across these studies.

Side products from photolytic generation of H_2SO_4 that enhance nucleation were suggested by Berndt et al. (2008), however, Sipila et al. (2010) found no difference between nucleation rates whether H_2SO_4 was produced photolytically or taken from a bulk source. Since then, the Sipila et al. (2010) nucleation rates have been seen to be many orders of magnitude too high for
15   the putative binary system (i.e., extrapolation of the present results, the Zollner et al. (2012) bulk-liquid data, results from the CLOUD experiment (Kirkby et al., Kurten et al. 2017) and Yu et al. (2017).) Since the Sipila et al. (2010) data largely overlaps the Benson et al. (2011) and Berndt et al. (2014) data, it probably also suffers from amine contaminants at the pptv-level.

The total particle number strongly depended on relative humidity with RH^4 and RH^6 power relationships over RH ranges of
20   15 to 35 % and 40 to 77%, respectively. The CLOUD 298 K data reported by Kurten et al. (2017) shows a power dependency of 4 on RH from 40 to 75 % at 298 K in rough agreement with the present results. Yu et al. reported a nucleation rate that depended linearly on RH that seems to be out of line with these other data sets.

A nearly linear dependence of N_p on added NH_3 was found which is also reflected in several other studies (Kirkby et al., Kurten et al., Benson et al.). This departs from the bulk-liquid experiments of Glasoe et al. who report a 1.6 NH_3-power
25   dependency and the ACDC model predicts a power dependency of 2 to 3 (Kurten et al., 2017), albeit at lower H_2SO_4. At constant NH_3, we found power dependencies on H_2SO_4 for N_p of about 3.5 which is close to that found by Glasoe et al. (2015) and somewhat larger than the CLOUD data (H_2SO_4-power dependency of 2.6.) A linear dependence on ammonia is consistent with nucleation initiated by sulfamic acid, as outlined by Lovejoy and Hanson (1996).

The model simulations with NH_3-H_2SO_4 thermodynamic schemes NH3_I and NH3_II (Hanson et al. 2017) resulted in N_p
30   that exceeded experiment for a large set of conditions. With the simulations serving as a bridge between these two experiments, we conclude that the present experimental data and the Glasoe et al. NH_3-H_2SO_4 results do not agree. Glasoe et al. discussed the discrepancies between their NH_3-H_2SO_4 results and those of Ball et al. and Zollner et al., but now, since the Glasoe et al. data are higher than the latter two as well as for much of the present results, we conclude that the Glasoe et al. NH_3 results are biased high. Finally, the putative agreement between Glasoe et al. and the 292 K 4 pptv NH_3 data from

CLOUD (demonstrated in Fig. 4 of Kurten et al. 2016) should not be a validation of these two sets of NH_3-H_2SO_4 nucleation rates.

In hindsight we can postulate a possible avenue for an amine contamination in the Glasoe et al. ammonia experiments: several amino-compounds were studied in succession with the same dynamic dilution system and ammonia experiments

5 were performed in between amine experiments. Measurements in the ammonia-sulfuric acid system would be most vulnerable to the presence of small amounts of holdover amines. Note that in the present experimental setup, there were separate dynamic dilution systems for ammonia and for dimethylamine.

Additions of dimethylamine resulted in large abundances of particles which limited the range of conditions we were able to study. The number densities are such that a model with proper treatments of coagulation and cluster- cluster collisions is

10 needed to fully interpret the results. Nonetheless, the experimental results are in decent agreement with model simulations using the dimethylamine thermodynamic scheme (DMA_I, Hanson et al., 2017) that best captured the Glasoe et al. (2015) dimethylamine-H_2SO_4 experimental results. We found low RH dependencies when dimethylamine was added in line with expectations but it should be emphasized that the linearity of the RH dependence of N_p is a preliminary finding and coagulation effects on these N_p values need to be investigated with a proper coagulation simulation.

15 Atmospheric implications of the present work are of a qualitative nature. The current work suggests that nucleation rates in the NH_3-H_2SO_4 system are still uncertain and need further experimental investigation. Furthermore, we conclude that the nucleation rate expression eq. 3 of Glasoe et al. (2015) likely overestimates nucleation in the ammonia-sulfuric acid system. On the other hand, as alluded to in the previous paragraph, the current work is consistent with the Glasoe et al. dimethylamine-H_2SO_4 results. Also, the much-predicted low RH dependency for dimethylamine-H_2SO_4 nucleation finds

20 experimental corroboration here. Finally, even if the reaction of HO_2 with SO_2 occurs with a rate coefficient of 1×10^{-16} cm^3 s^{-1}, it is probably an insignificant source of atmospheric hydroxyl radicals and oxidized sulfur compounds.

In the future, a series of measurements of particles with added dimethylamine at fractional pptv levels are planned to better determine H_2SO_4 and amine dependencies. We also plan to study the relative humidity dependence of ammonia-induced H_2SO_4 nucleation as well as variations of temperature on both amine- and ammonia-addition nucleation. In the long term,

25 the system developed here will be used in particle growth studies where nm-diameter particles prepared in the Glasoe et al. apparatus are directed through PhoFR along with target organic compounds.

Author contribution.

30 HA and JV built the particle detector and performed preliminary experiments, MA helped design and carry out experiments, SM carried out added-NH_3 experiments and helped with the manuscript, JK helped develop the photochemical module, and DH developed and ran the simulations, developed and carried out experiments and prepared the manuscript with contributions from all co-authors. The authors declare that they have no conflict of interest.

Atmospheric
Chemistry
and Physics
Discussions

Open Access

10 References

Almeida, J., S. Schobesberger, A. Kurten, I. K. Ortega, O. Kupiainen-Maatta, A. P. Praplan, A. Adamov, et al. "Molecular Understanding of Sulphuric Acid-Amine Particle Nucleation in the Atmosphere," *Nature (London, United Kingdom)* 502 (7471): 359-363. doi:10.1038/nature12663. 2013.

Ball, S. M., D. R. Hanson, F. L. Eisele, and Peter H. McMurry. "Laboratory Studies of Particle Nucleation - Initial Results

15 for H2SO4, H2O, and NH3 Vapors." *J Geophys Res* 104 (D19): 23, 718, 1999.

Benson, D. R., J. H. Yu, A. Markovich, and S. -H Lee. "Ternary Homogeneous Nucleation of H2SO4, NH3, and H2O Under Conditions Relevant to the Lower Troposphere." *Atmos Chem Phys* 11 (10): 4755-4766. doi:10.5194/acp-11-4755-2011, 2011.

Berndt, T., F. Stratmann, M. Sipilae, J. Vanhanen, T. Petaejae, J. Mikkilae, A. Gruener, et al. "Laboratory Study on New

20 Particle Formation from the Reaction OH + SO2: Influence of Experimental Conditions, H2O Vapour, NH3 and the Amine Tert-Butylamine on the overall Process." *Atmos Chem Phys* 10 (15): 7101-7116. doi:10.5194/acp-10-7101-2010., 2010.

Burrows, J. P., D. I. Cliff, G. W. Harris, B. A. Thrush, and J. P. T. Wilkinson. "Atmospheric Reactions of the HO_2 Radical Studied Buy Laser MRS." *Proc Royal Soc of London. Ser A,* 368: 463-481, 1979.

Coffman, D. J. and D. A. Hegg. "A Preliminary Study of the Effect of Ammonia on Particle Nucleation in the Marine

25 Boundary Layer." *J. Geophys. Res., [Atmospheres]* 100 (D4): 7147-7160. doi:10.1029/94JD03253, 1995.

Ehrhart, S. et al.: Comparison of the SAWNUC model with CLOUD measurements of sulphuric acid-water nucleation, J. Geophys. Res. Atmos., 121, 2016.

Febo, A., Perrino, C., Sparapani, R. and Gherardi, M.: Evaluation of a High-Purity and High-Stability Continuous Generation System for Nitrous Acid, Environ. Sci. Tech., 29, 2390-2395, 1995.

30 Friese, E. and Ebel, A.: Temperature Dependent Thermodynamic Model of the System H+−NH4+−Na+−SO42−−NO3−−Cl−−H2O, J Phys Chem A, 114, 11595-11631, 10.1021/jp101041j, 2010.

Freshour, N., K. K. Carlson, Y. A. Melka, S. Hinz, B. Panta, and D. R. Hanson "Quantifying Amine Permeation Sources with Acid Neutralization: Calibrations and Amines Measured in Coastal and Continental Atmospheres." *Atmos. Meas. Tech.* 7: 3835-3861, 2014.

Glasoe, W. A., K. Volz, B. Panta, N. Freshour, R. Bachman, D. R. Hanson, P. H. McMurry, and C. N. Jen. "Sulfuric Acid Nucleation: An Experimental Study of the Effect of Seven Bases." *J. Geophys. Res. D.* 120, 2015.

Hanson, D. R., I. Bier, B. Panta, C. N. Jen, and P. H. McMurry. "Computational Fluid Dynamics Studies of a Flow Reactor: Free Energies of Clusters of Sulfuric Acid with NH3 and Dimethylamine." *J. Phys. Chem. A* 121 (20): 3976, 2017.

Henschel, H., T. Kurten, and H. Vehkamaki "Computational Study on the Effect of Hydration on New Particle Formation in the Sulfuric Acid/Ammonia and Sulfuric Acid/Dimethylamine Systems," *J. Phys. Chem. A* 120, 1886-1896. doi:10.1021/acs.jpca.5b11366, 2016.

Intergovernmental Panel on Climate Change (2013), Climate Change 2013: IPCC 5th Assessment Report (AR5), Edited, 2013.

Jiang, J., M. Chen, C. Kuang, M. Attoui, and P. H. McMurry. "Electrical Mobility Spectrometer using a Diethylene Glycol Condensation Particle Counter for Measurement of Aerosol Size Distributions Down to 1 Nm." *Aerosol Science and Technology* 45 (4): 510-521. doi:10.1080/02786826.2010.547538, 2011.

Kirkby, J., et al. "Role of Sulphuric Acid, Ammonia and Galactic Cosmic Rays in Atmospheric Aerosol Nucleation." *Nature* 476: 429-433. doi:10.1038/nature10343, 2011.

Kreyling, W. G., Semmler-Behnke, M. and Moller, W.: Ultrafine Particle-Lung Interactions: Does Size Matter? J. Aerosol Medicine, 19, 74-83, 10.1089/jam.2006.19.74, 2006.

Kuang, C., M. Chen, J. Zhao, J. Smith, P. H. McMurry, and J. Wang. "Size and Time-Resolved Growth Rate Measurements of 1 to 5 Nm Freshly Formed Atmospheric Nuclei." *Atmospheric Chemistry and Physics* 12 (7): 3573-3589. doi:10.5194/acp-12-3573-2012, 2012.

Kulmala, M., H. Vehkamaki, T. Petaja, M. Dal Maso, A. Lauri, V. -M Kerminen, W. Birmili, and P. H. McMurry. "Formation and Growth Rates of Ultrafine Atmospheric Particles: A Review of Observations." *Journal of Aerosol Science* 35 (2): 143-176. doi:10.1016/j.jaerosci.2003.10.003, 2004.

Kürten, A., C. Williamson, J. Almeida, J. Kirkby, and J. Curtius. "On the Derivation of Particle Nucleation Rates from Experimental Formation Rates." *Atmospheric Chemistry and Physics* 15 (8): 4063-4075. doi:10.5194/acp-15-4063-2015, 2015.

Kürten, A. et al. "Experimental Particle Formation Rates Spanning Tropospheric Sulfuric Acid and Ammonia Abundances, Ion Production Rates, and Temperatures," *J. Geophys. Res.* 121 (20): 12,400. doi:10.1002/2015JD023908, 2016.

Kürten, A., et al., J. Curtius, P. H. McMurry "New Particle Formation in the Sulfuric Acid–dimethylamine–water System: Reevaluation of CLOUD Chamber Measurements and Comparison to an Aerosol Nucleation and Growth Model" *Atmos. Chem. Phys.* doi:10.5194/acp-18-845-2018, 2018.

16

Kurten, T., V. Loukonen, H. Vehkamaki, and M. Kulmala. "Amines are Likely to Enhance Neutral and Ion-Induced Sulfuric Acid-Water Nucleation in the Atmosphere More Effectively than Ammonia." *Atmospheric Chemistry and Physics* 8 (14): 4095-4103. doi:10.5194/acp-8-4095-2008, 2018.

Larriba, A., Hogan, C. and de lamora, J.: The Mobility–Volume Relationship below 3.0 nm Examined by Tandem Mobility–Mass Measurement, Aerosol Science and Technology, 45, 453-467, 2010.

Lovejoy, E. R., Hanson, D. R. and Huey, L. G.: Kinetics and Products of the Gas-Phase Reaction of SO3 with Water, J. Phys. Chem., 100, 19911-19916, 1996.

Lovejoy, E. R., Hanson, D. R.: Kinetics and Products of the Reaction SO3 + NH3 + M, J. Phys. Chem., 100, 4459, 1996.

McMurry, P. H. "New Particle Formation in the Presence of an Aerosol: Rates, Time Scales, and Sub-0.01 Um Size Distributions," *Journal of Colloid and Interface Science* 95 (1): 72-80. doi:10.1016/0021-9797(83)90073-5, 1983.

McMurry, P. H., M. Fink, H. Sakurai, M. R. Stolzenburg, R. L. Mauldin III, J. Smith, F. Eisele, et al. "A Criterion for New Particle Formation in the Sulfur-Rich Atlanta Atmosphere." *J. Geophys. Res.,* 110 (D22): D22S02/10. doi:10.1029/2005JD005901, 2005.

Nadykto, A. and F. Yu. "Amine's in the Earth's Atmosphere: A Density Functional Theory Study of the Thermochemistry of Pre-Nucleation Clusters," *Entropy* 13: 554-569, 2011.

Nel, A. "Air Pollution-Related Illness: Effects of Particles." *Science* 308 (5723): 804-806. doi:10.1126/science.1108752, 2005.

Ortega, I. K., O. Kupiainen, T. Kurten, T. Olenius, O. Wilkman, M. J. McGrath, V. Loukonen, and H. Vehkamaki. "From Quantum Chemical Formation Free Energies to Evaporation Rates." *Atmospheric Chemistry and Physics* 12 (1): 225-235. doi:10.5194/acp-12-225-2012, 2012.

Panta, B, W A Glasoe, J H Zollner, K K. Carlson, and D. R. Hanson "Computational Fluid Dynamics of a Cylindrical Nucleation Flow Reactor with Detailed Cluster Thermodynamics," *J Phys Chem A* 116: 10122-10134. doi:10.1021/jp302444y, 2012.

Payne, W. A., L. J. Stief, and D. D. Davis. "A Kinetics Study of the Reaction of HO_2 with SO_2 and NO;" *J. Am. Chem. Soc.* 95: 7614-7619, 1973.

Graham, R.A., A M Winer, R Atkinson, and J Pitts Jr. "Rate Constants for the Reaction of HO_2 with HO_2, SO_2, CO, N_20, Trans-2-Butene, and 2,3-Dimethyl-2-Butene at 300 K." *J. Phys. Chem.* 83, 1979.

Sipilae, M., T. Berndt, T. Petaejae, D. Brus, J. Vanhanen, F. Stratmann, J. Patokoski, et al "The Role of Sulfuric Acid in Atmospheric Nucleation." *Science* 327: 1243-1246. doi:10.1126/science.1180315, 2010.

Sörgel, M., E. Regelin, H. Bozem, J. -M Diesch, F. Drewnick, H. Fischer, H. Harder, et al. "Quantification of the Unknown HONO Daytime Source and its Relation to NO2." *Atmospheric Chemistry and Physics* 11 (20): 10433-10447. doi:10.5194/acp-11-10433-2011, 2011.

Viisanen, Y., M Kulmala, and A Laaksonen. "Experiments on Gas-Liquid Nucleation of Sulfuric Acid and Water." *Journal of Chemical Physics* 107 (3): 920-926. doi:10.1063/1.474445, 1997.

Atmospheric
Chemistry
and Physics
Discussions

Verheggen, B. and M. Mozurkewich. "Determination of Nucleation and Growth Rates from Observation of a SO2 Induced Atmospheric Nucleation Event." *J Geophys Res* 107, doi:10.1029/2001JD000683, 2002.

Wexler, A. S. and S. L. Clegg. "Atmospheric Aerosol Models for Systems Including the Ions H+, NH4+, Na+, SO42−, NO3−, Cl−, Br−, and H2O." *J Geophys Res* 107 (D14): 4207. doi:10.1029/2001JD000451, 2002.

5   Wyslouzil, B. E., J. H. Seinfeld, R. C. Flagan, and K. Okuyama. "Binary Nucleation in Acid-Water Systems. II. Sulfuric Acid-Water and a Comparison with Methanesulfonic Acid-Water." *Journal of Chemical Physics* 94 (10): 6842-6850. doi:10.1063/1.460262, 1991.

Yu, H., L Dai, Y Zhao, V P. Kanawade, S N. Tripathi, X Ge, M Chen, and S.-Hu Lee. "Laboratory Observations of Temperature and Humidity Dependencies of Nucleation and Growth Rates of Sub-3 nm Particles." *J. Geophys. Res.:*
10   *Atmospheres* 122 (3): 1919-1929. doi:10.1002/2016JD025619, . 2017.

Yu, H, R McGraw, and S-H Lee. "Effects of Amines on Formation of Sub-3 Nm Particles and their Subsequent Growth." *Geophysical Research Letters* 39. doi:10.1029/2011GL050099, 2012.

Zollner, J. H., W. A. Glasoe, B. Panta, K. K. Carlson, P. H. McMurry, and D. R. Hanson. "Sulfuric Acid Nucleation: Power Dependencies, Variation with Relative Humidity, and Effect of Bases," *Atmospheric Chemistry and Physics* 12 (10): 4399-
15   4411. doi:10.5194/acp-12-4399-2012, 2012.

20

25

30

Atmospheric
Chemistry
and Physics
Discussions

Figures and captions.
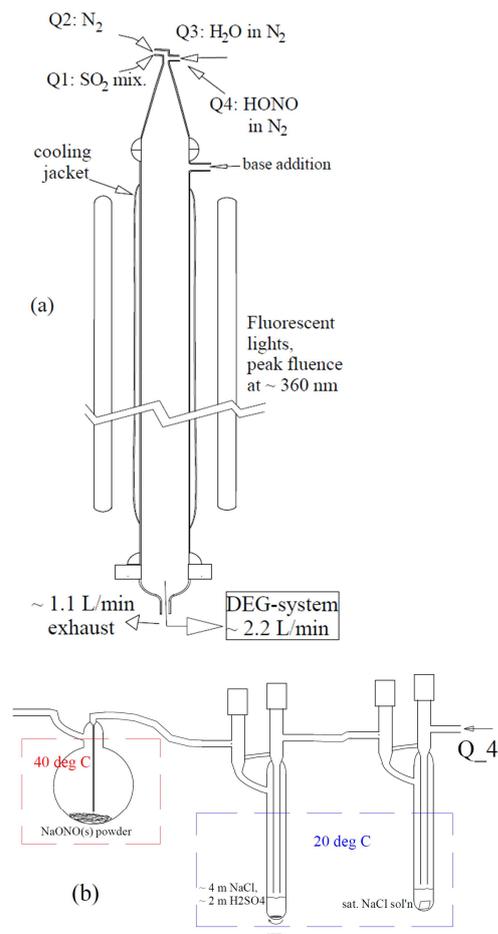
5 **Fig. 1 (a) PhoFR schematic and (b) HONO source. The average flow velocity of 2.8 cm/s yields an average residence time in PhoFR of approximately 45 s. The concentrations listed in (b) are in molal (mole per kg H₂O).**

Atmospheric
Chemistry
and Physics
Discussions
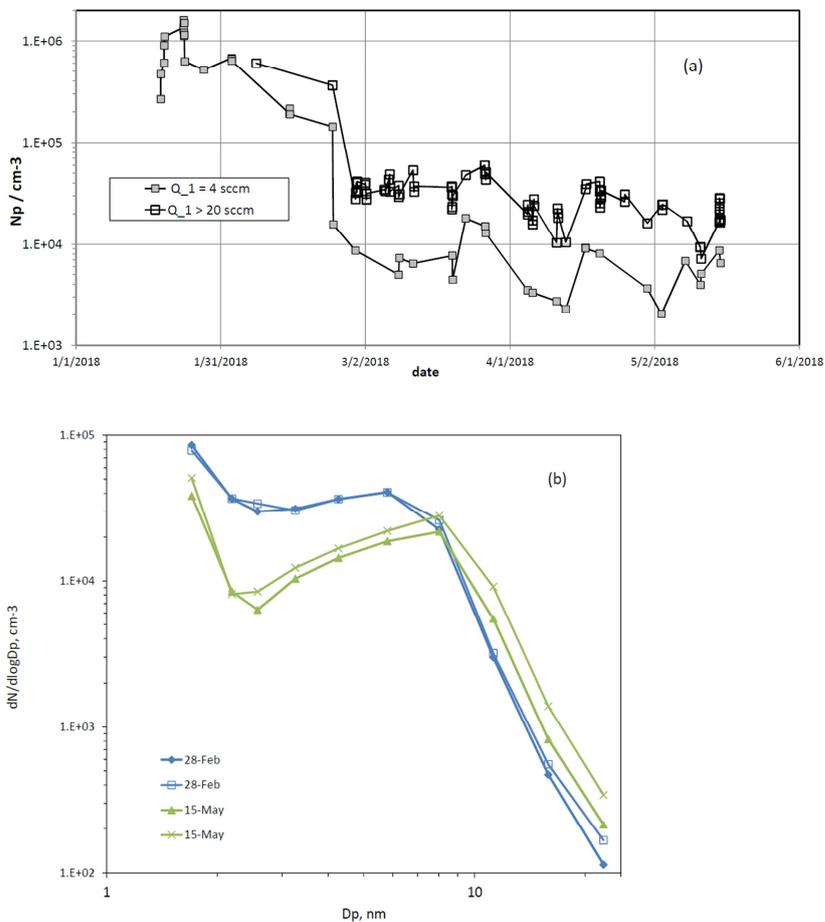
Fig. 2. (a) Number of large particles for baseline HONO (Q$_4$=4.2 sccm: [HONO] = 5x10^{11} cm^{-3}) plotted vs. time for two different SO$_2$ levels, equivalent to 2 and >10 ppmv. (b) Measured size distributions for the high SO$_2$ conditions just after the mesh was installed, Feb. 23rd, and late in the time period depicted in (a).

Atmospheric
Chemistry
and Physics
Discussions
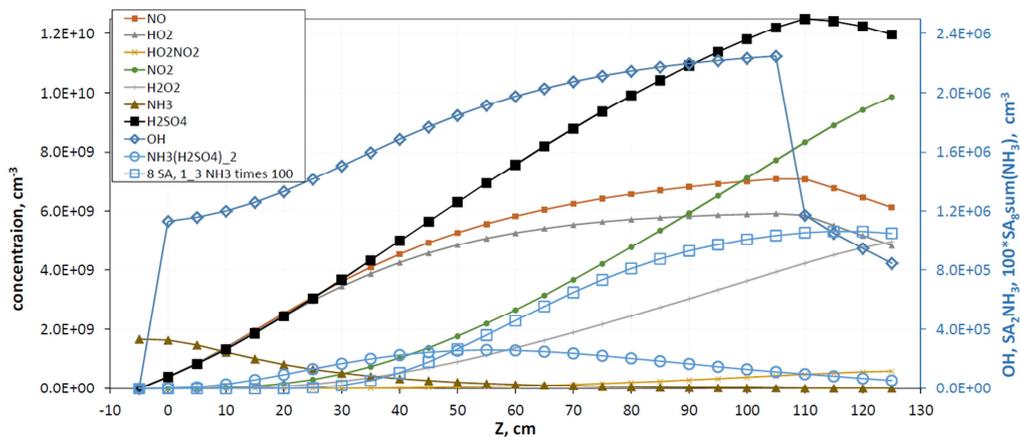
Fig. 3. Model simulation for [HONO]= 5×10^{11} cm^{-3}, [SO$_2$] = 4×10^{14} cm^{-3}. Concentrations of NO through H$_2$SO$_4$ are plotted on the left axis; concentrations of OH, and the (H$_2$SO$_4$)$_2$NH$_3$ and (H$_2$SO$_4$)$_8$(NH$_3$)$_{1,2,3}$ clusters on the right axis (the latter clusters were summed over NH$_3$ content and multiplied by 100). These simulations are equivalent to experimental conditions of Q$_4$=4.0 sccm, Q$_1$
5 **= 32 sccm and added NH$_3$ at 70 pptv. The lighted section is from 0 to 110 cm. At 110 cm HONO photolysis ceases and [OH] (right axis) drops to a level supplied by HO$_2$ + NO.**

21
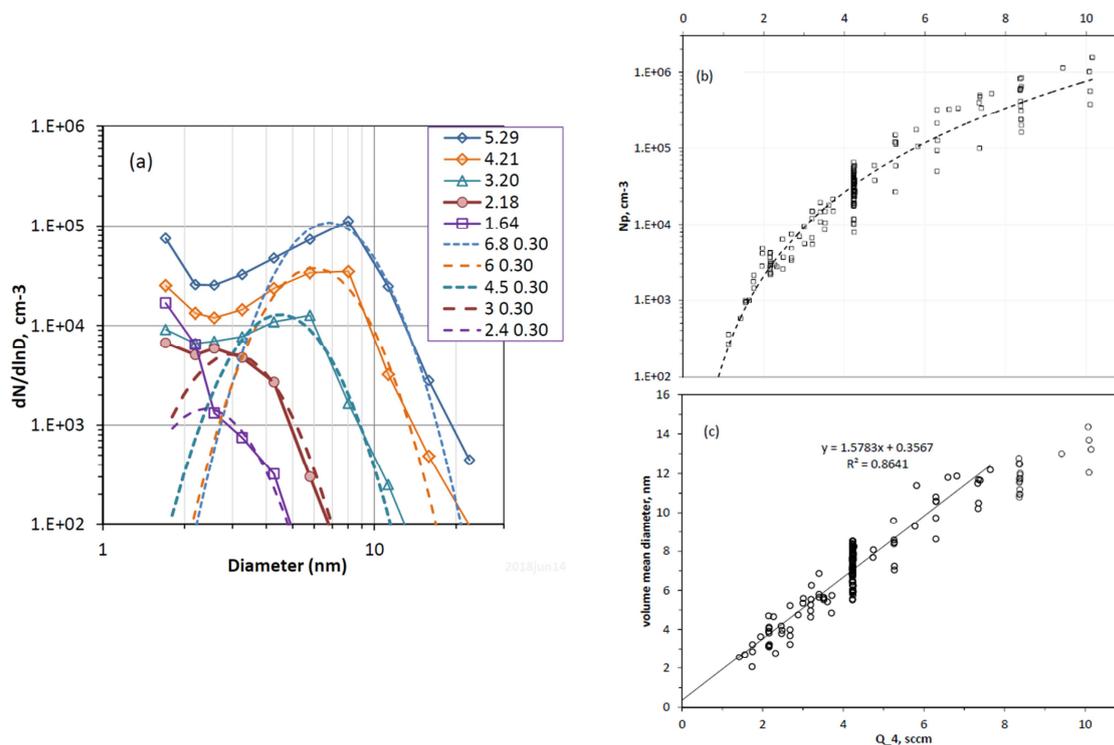
Fig. 4. **(a) Measured size distributions as a function of Q$_4$, the flow rate through the HONO generator. Log-normal distributions manually fitted to the leading edge are shown as the dashed lines. Note that raw count rates at the smallest size for the three lowest**
5 **Q$_4$ are roughly 0.1 s^{-1} and, statistically, they are not significantly different. This is slightly above the background count rate of ~0.05 s^{-1}. (b) Number of large particles as a function of Q$_4$, the HONO-laden flow rate. RH was 52 %, T = 296 K, and [SO$_2$] > 2.5x10^{14} cm^{-3}. For reference, Q$_4$ = 4 sccm results in a modeled value of ~ 4x10^9 cm^{-3} for H$_2$SO$_4$ at Z = 35 cm and R = 0 (the center of the reactor; see Fig. 3.) (c) Volume mean diameter of the particles in the leading edge of the particle distributions, D$_{V,le}$ = D$_{le}$*exp(1.5lnσ^2). D$_{le}$ and lnσ from those distributions that had a local minimum between the smallest particles and the peak at**
10 **large diameters and thus were able to be fit.**
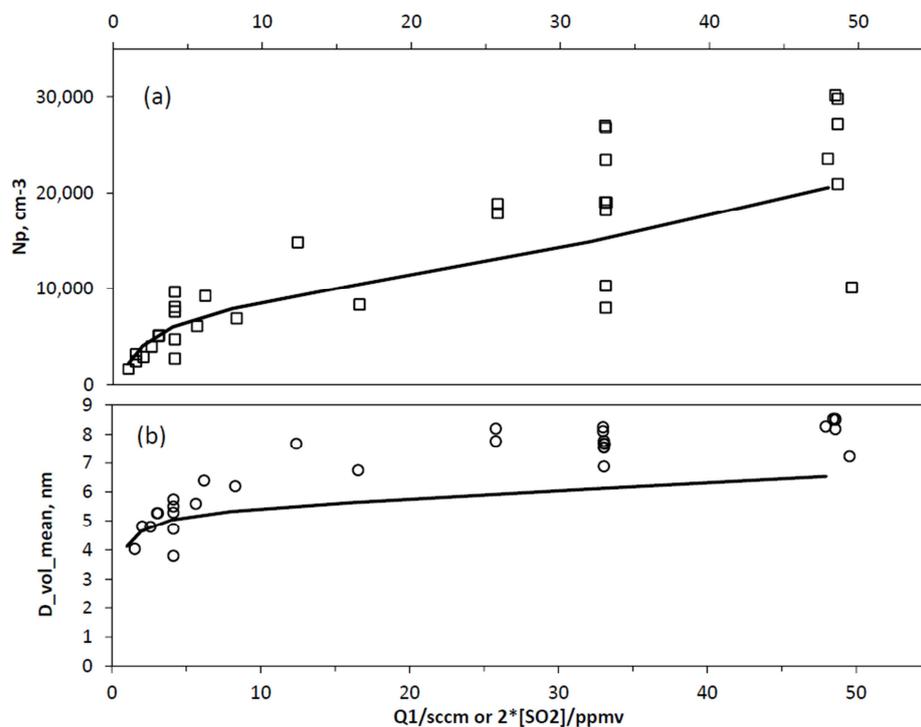
Fig. 5 (a) Number of large particles and (b) volume mean diameter of the leading edge mode plotted vs. flow rate of SO$_2$ mixture. Q$_4$, the HONO-source flow rate, was 4.2 sccm which results in roughly 5x10^{11} cm^{-3} [HONO] in PhoFR. For reference, an SO$_2$ mixture flow rate of 32 sccm results in an [SO$_2$] of 4x10^{14} cm^{-3} in PhoFR (about 16 pptv). The orange lines are model values for N$_p$
5 **and size with 70 pptv NH$_3$ entering the flow reactor and a k3x5 (HO$_2$ + SO$_2$) rate coefficient of 3x10^{-17} cm^3/s. The simulated size has 1.3 nm (to take into account initial cluster size of ~ 1 nm and the mobility to mass size difference of 0.3 nm. de La Mora et al.) added to the growth due to H$_2$SO$_4$ exposure as discussed above.**
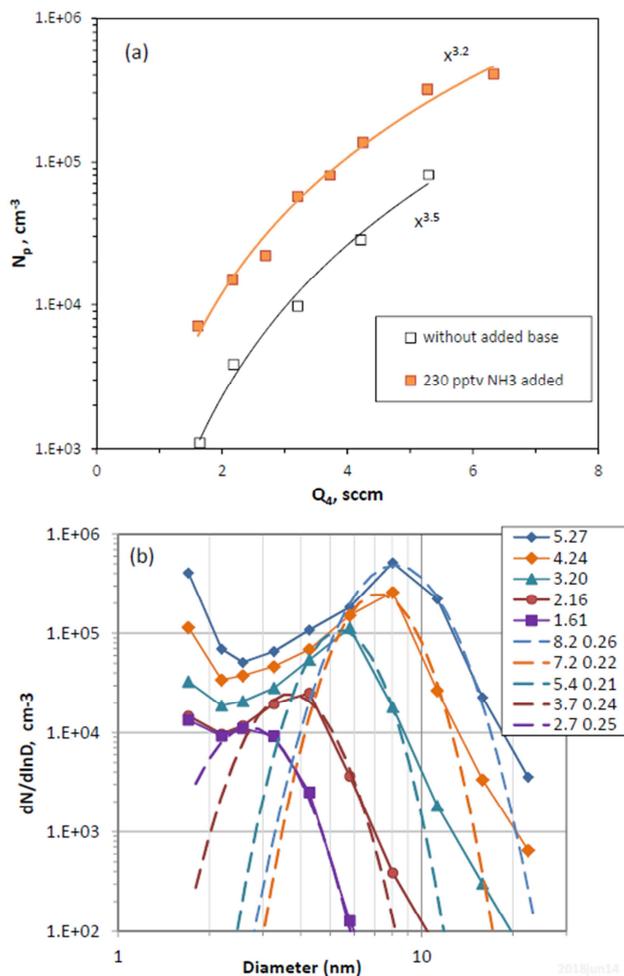
Fig. 6 (a) N_p vs. Q_4 (i.e., HONO) and (b) particle size distributions with NH_3 present. In (b), the log-normal parameters are listed in the legend and were obtained from a fitting procedure except for the $Q_4 = 1.61$ sccm data.
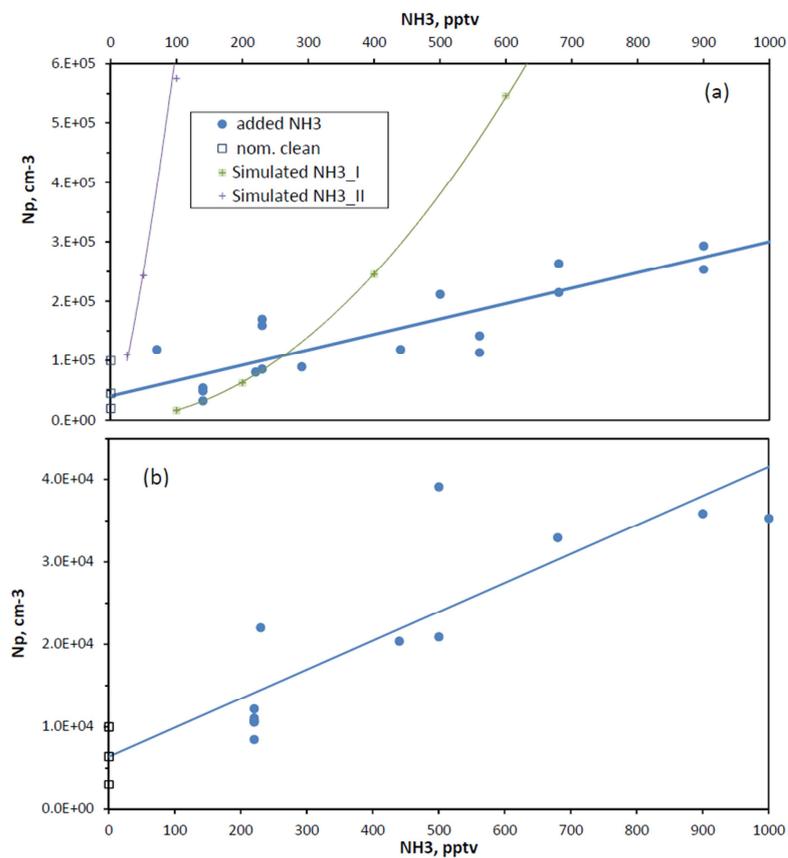
Fig. 7. Variation of N_p with added NH_3 for Q_4 of (a) 4.3 sccm and (b) 2.2 sccm. Simulated Np are shown in (a) for NH3_I and NH3_II thermodynamics. The range of measured N_p without added base are shown as the squares.

Atmospheric
Chemistry
and Physics
Discussions

Open Access
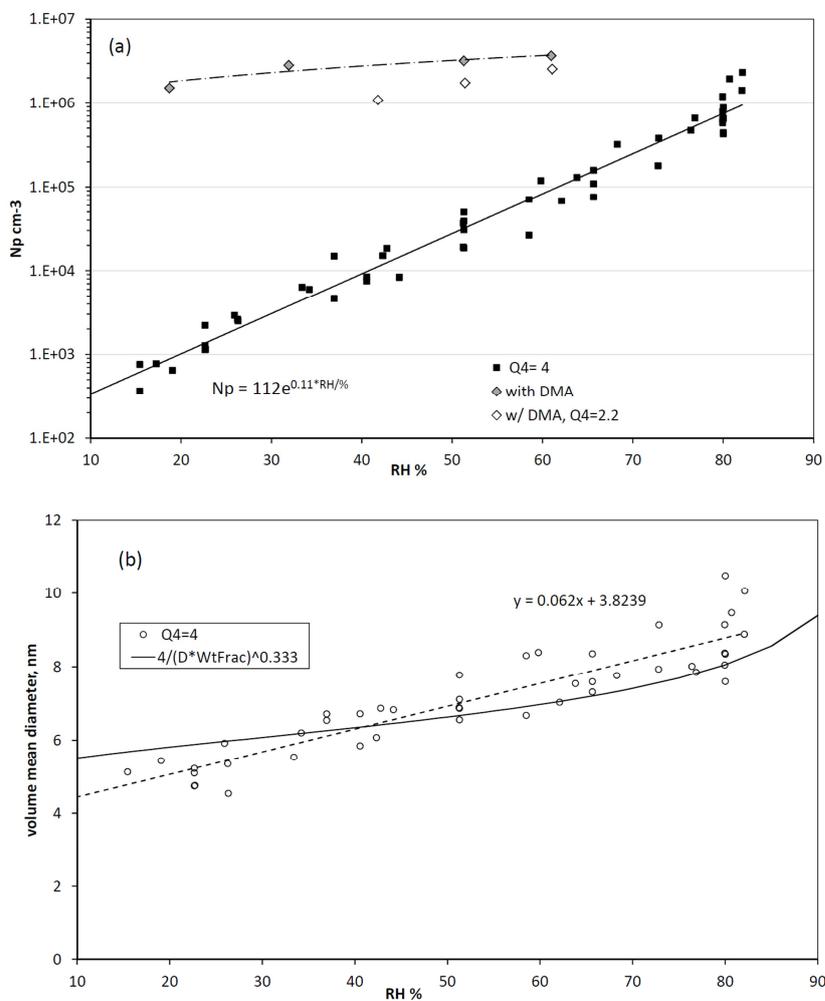
Fig. 8. Variation of (a) N_p and (b) $D_{V,le}$ with RH in % (RH determined by the fraction of flow through the water saturator, Q_3) Q_4 was 4.2 sccm and $Q_1 > 20$ sccm. Plot (a) also shows data with dimethyl amine added: at 2 pptv (filled diamonds) and data at a
5   lower $Q_4 = 2.1$ sccm and dimethyl amine at 5 pptv. In (b) a linear fit is shown as the dashed line (phenomenological) while the solid line is the diameter increase based on water uptake using bulk values for the density and mass fraction of H_2SO_4 as a function of RH (Wexler and Clegg, 2002).
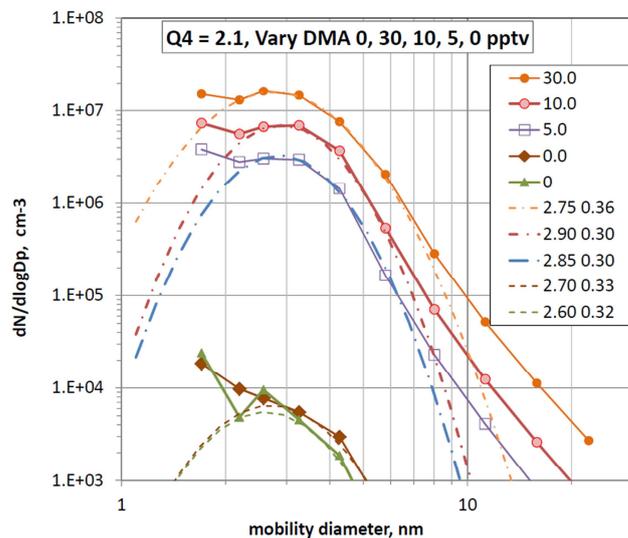
**Fig. 9 Size distributions as a function of added dimethyl amine.**
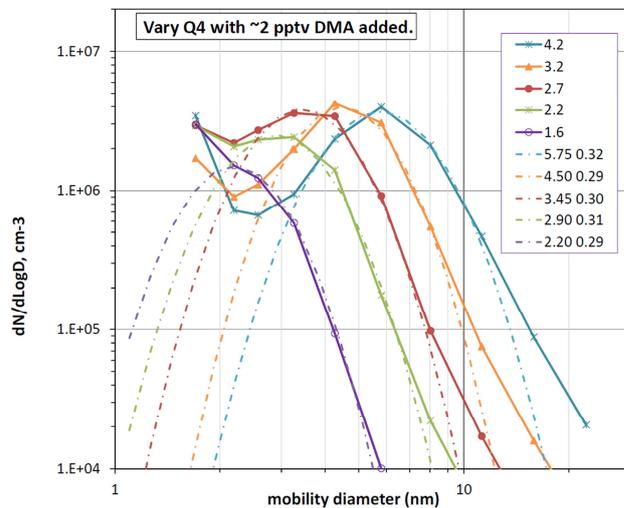
**Fig. 10. Size distributions as a function of HONO level.**
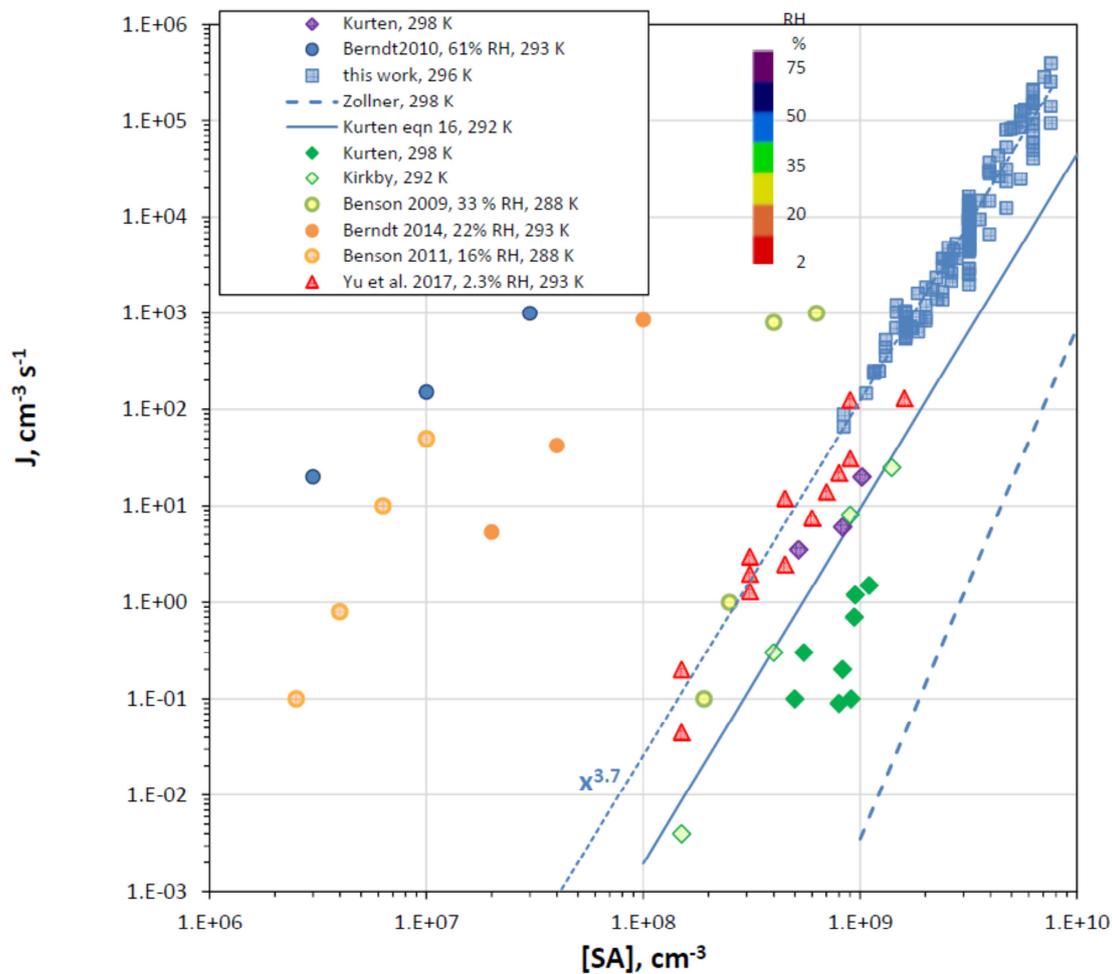
Fig. 11: Comparison of results from previous work (all photolytic H$_2$SO$_4$ production except Zollner et al., 2012) for nominally clean conditions. RH color-coding was applied to the points and temperatures are indicated in the legend.

5